# Nonunity permeability in metamaterial-based GaInAsP/InP multimode interferometers

**T. Amemiya,[1,*] T. Shindo,[2] D. Takahashi,[2] S. Myoga,[2] N. Nishiyama,[2] and S. Arai[1,2]**

[1]*Quantum Nanoelectronics Research Center, Tokyo Institute of Technology, Tokyo 152-8552, Japan*

[2]*Department of Electrical and Electronic Engineering, Tokyo Institute of Technology, Tokyo 152-8552, Japan*

**Corresponding author: amemiya.t.ab@m.titech.ac.jp*

Received March 30, 2011; revised May 14, 2011; accepted May 14, 2011;
posted May 16, 2011 (Doc. ID 145048); published June 15, 2011

We demonstrated an InP-based optical multimode interferometer (MMI) combined with metamaterials consisting of minute split-ring resonators (SRRs) arrayed on the MMI. The MMI could operate at an optical fiber communication wavelength of 1.5 $\mu$m. Magnetic resonance occurred between the SRR metamaterial and light at 1.5 $\mu$m, and the relative permeability of the metamaterial increased to 2.4 around this wavelength. This result shows that it is possible to use new materials with nonunity permeability to construct semiconductor-based photonic devices. © 2011 Optical Society of America

*OCIS codes:* 130.0130, 160.3918, 130.5990.

The relative permeability $\mu$ of every natural material is 1 at optical frequencies because the magnetization of the material cannot follow the alternating magnetic field of light. Therefore, with conventional photonic devices [1,2], we cannot directly affect the magnetic component of light; we must make do with affecting only the electric component, which is feasible by using semiconductors with different permittivity values. However, this limits our ability to control electromagnetic waves at will in photonic systems.

Recently, controlling the optical properties of materials using metallic subwavelength structures has attracted growing interest [3–5]. Such artificial materials, called *metamaterials*, give us the possibility to control the permeability of materials at optical frequencies.

It is a promising challenge to introduce the concept of metamaterials into semiconductor-based photonic devices. Using metamaterials, we will be able to create novel optical functionalities to open up new fields, such as *metaphotonics*. For example, it is possible in theory to achieve sophisticated manipulation of light, such as slowing and trapping light signals in optical waveguides [6–8].

In this Letter, we demonstrate an InP-based optical waveguide device combined with a metamaterial to show the possibility of permeability control in semiconductor photonic devices. Figure 1 shows a schematic illustration of our device consisting of a GaInAsP/InP optical MMI and metal SRRs arrayed on the MMI. Each SRR acts as an artificial magnetic atom, and, therefore, the SRR array operates as a magnetic metamaterial layer. We used the MMI, instead of a single-mode waveguide, as the stage of interaction between SRRs and light. A strong interaction can be expected in the MMI because the confinement factor of the SRR region is larger for multimode light than for single-mode light.

In this structure, if the input TE-mode light has a frequency matched to SRR resonance, the SRR produces a circular current in response to an incident magnetic flux, thereby producing its own flux to enhance or oppose the incident field. Consequently, the SRR array operates as a metamaterial layer with nonunity permeability ($\mu \neq 1$) [9–11].

We fabricated the device for use at 1.5 $\mu$m wavelength (matched to low-loss optical fiber communication) and confirmed the magnetic interaction between the SRR metamaterial layer and the light that traveled in the MMI. The fabrication process of the device is as follows. First, four undoped layers, i.e., a $Ga_{0.23}In_{0.77}As_{0.5}P_{0.5}$ core layer ($\lambda_g = 1.22\,\mu$m, 200 nm thick), an InP layer (20 nm thick), an $Al_{0.48}In_{0.52}As$ etch-stop layer (5 nm thick), and an InP cladding layer (400 nm thick) were grown in this order on a (100) oriented semi-insulating InP substrate by organometallic vapor phase epitaxy. On the surface of the cladding layer, an SRR array (consisting of 5 nm thick Ti and 20 nm thick Au) was formed using electron-beam (EB) lithography and a lift-off process. Figures 2(a) and 2(b) show the oblique images of the SRR array observed with a scanning electron microscope (SEM). A *4-cut* single SRR [Fig. 2(a)] structure was used in the SRR array because it has a high resonant frequency due to its small gap capacitance [12]. The size of the SRR was designed for use at a band frequency of 1.5 $\mu$m (193 THz). In this study, we made SRRs of different sizes ranging from $300 \times 300$ to $500 \times 500$ nm (inner size of the square SRR ring). Both the width and gap of the SRR metal region were set to 75 nm. After the formation of the SRR array, an $SiO_2$ mask (100 nm thick) for the MMI pattern was formed on the device with plasma-enhanced chemical

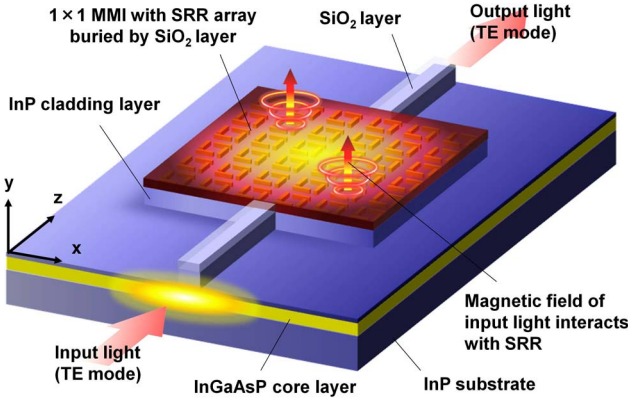


Fig. 1. (Color online) Waveguide-based multimode interferometer (GaInAsP/InP $1 \times 1$ MMI) and metamaterial region consisting of metal SRR array attached onto the MMI.

 

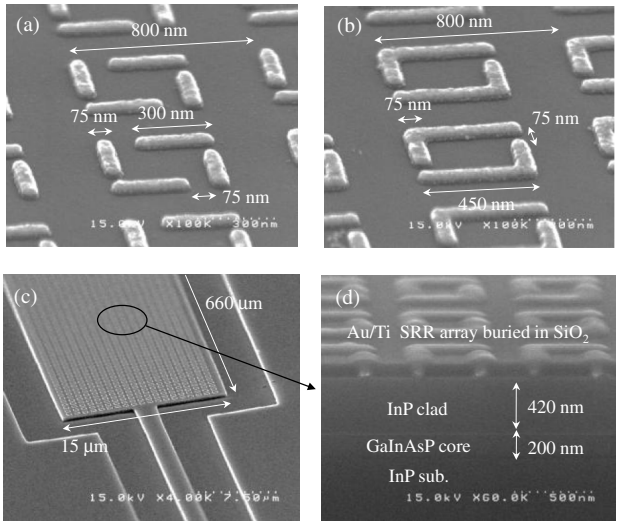


Fig. 2. (a) Enlarged oblique views of 4-cut SRRs, and (b) 2-cut SRRs observed with scanning electron microscopy; (c) Oblique view of completed device, and (d) cross-sectional view of $300 \times 300$ nm SRRs buried in the $SiO_2$ layer.

vapor deposition and EB lithography. With the $SiO_2$ mask, the $1 \times 1$ MMI structure was formed using $CH_4/H_2$ reactive-ion etching. The width and length of the MMI were set to 15 and 660 $\mu$m, respectively. Figures 2(c) and 2(d), respectively, show oblique and cross-sectional SEM images of the MMI region with $300 \times 300$ nm SRRs.

In addition to these experimental samples, we also made control samples with SRRs consisting of *2-cut* Au/Ti square rings [Fig. 2(b)] with the same side length as that of the *4-cut* SRR. This *2-cut* SRR has a resonant frequency far lower than 193 THz (about 100 THz), so it does not interact with 1.5 $\mu$m light.

To examine the magnetic interaction between the SRRs and the light traveling in the MMI, we measured the transmission spectra for TE-mode light. The SRR resonance produces a permeability change, and this will decrease the transmittance of the MMI with two effects. First, the resonance changes the real part of the permeability, thereby changing the phase of light, and this will weaken the coupling between the input and output ports of the MMI. Second, the resonance also produces the imaginary part of the permeability, and this will increase the absorption loss of light in the MMI.

In the measurements, the light was emitted from a tunable laser to the device through a polarization controller. The wavelength was varied in the range of 1420–1575 nm. To clarify the effect of the magnetic interaction, we took the ratio of the transmission intensity for the control samples (with *2-cut* SRRs) to that for the experimental samples (with *4-cut* SRRs). This ratio shows an intrinsic change in transmission intensity induced by the SRR resonance without including parasitic factors, such as wavelength-dependent ohmic loss in the SRR metal, lensed-fiber coupling loss, and wavelength-dependent propagation characteristics in the MMI.

Figure 3 plots the measured transmission intensity ratio as a function of wavelength for devices with an SRR size of (a) $300 \times 300$ nm, (b) $350 \times 350$ nm, (c) $400 \times 400$ nm, and (d) $500 \times 500$ nm. The magnetic interaction was observed clearly in the device with

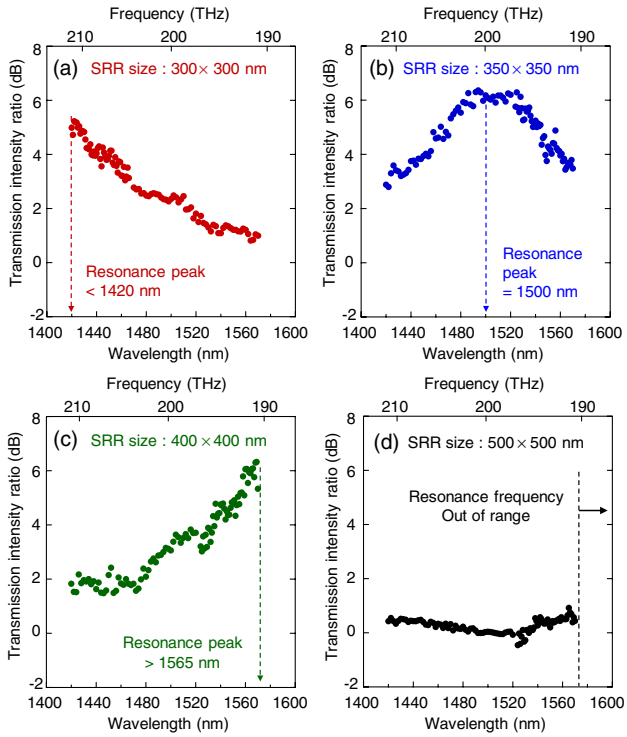


Fig. 3. (Color online) Transmission-intensity ratio (2-cut SRR/4-cut SRR) for devices with SRR size of (a) $300 \times 300$ nm, (b) $350 \times 350$ nm, (c) $400 \times 400$ nm, and (d) $500 \times 500$ nm as a function of wavelength from 1420 to 1575 nm, measured for TE-mode light.

$350 \times 350$ nm SRRs, as can be seen in Fig. 3(b) where the intensity ratio, induced by the SRR resonance, showed a peak at a wavelength of 1500 nm. This peak shifted toward a shorter and longer wavelength for smaller and larger SRRs, respectively [Figs. 3(a) and 3(c)], even though the wavelength for the peak was out of the measurement range. With $500 \times 500$ nm SRRs, the intensity ratio was almost 1 (= 0 dB) at this wavelength range, as can be seen in Fig. 3(d). This showed that no SRR resonance occurred at a wavelength of 1.5 $\mu$m. These wavelength-dependent and SRR-size-dependent transmission characteristics show that the magnetic field of light successfully interacted with the SRRs to produce magnetic resonance at an optical frequency.

The equivalent permeability and permittivity of the SRR array layer are a function of the wavelength. To know their values precisely, we must know both the intrinsic absorption loss and the phase shift of the propagating light in the device. However, we cannot extract each separately from the transmission data shown in Fig. 3. Therefore, we estimated the equivalent permittivity and permeability with theoretical calculations as follows: (1) We calculated the transmittance and reflectance of the SRR array sandwiched between InP, $SiO_2$ and air, using a 3D full-wave solver based on the finite element method; (2) With the transmittance and reflectance, we calculated the refractive index tensor (or permittivity and permeability tensors) of the SRR layer.

With the refractive index tensors of the SRR layer and GaInAsP/InP semiconductor layers, we calculated the transmission spectra of the MMI, using the transfer matrix method. The transfer matrix for each layer of

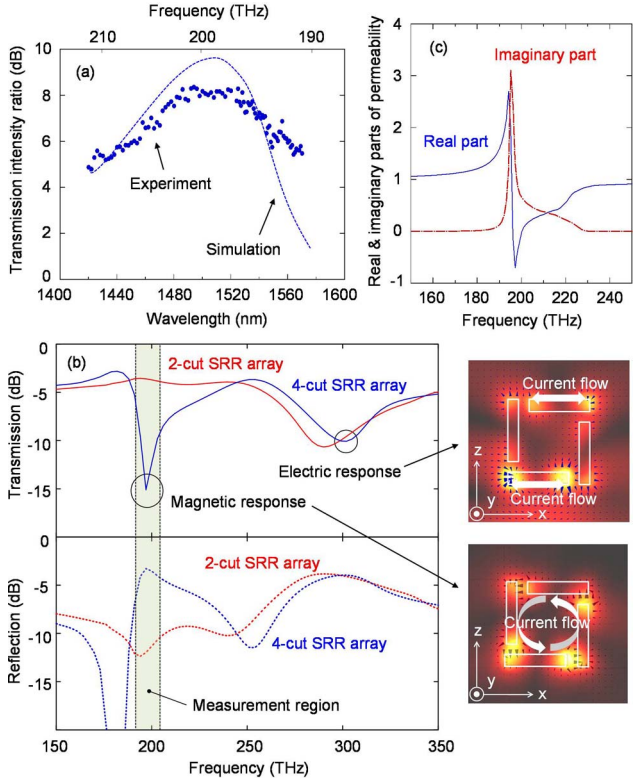


Fig. 4. (Color online) (a) Calculated transmission intensity ratio (dashed curve) compared with the measured data [closed circles, from Fig. 3(b)]. (b) Transmittance and reflectance estimated for a row of SRRs. Insets visualize distribution of electric field (magnitude and direction) in SRR at minimum transmission frequencies. (c) Effective permeability (real and imaginary parts) of SRR array.

the device can be obtained from Maxwell's equations, using the permittivity and permeability tensors [13]. We find from the transfer matrices that electric field $E_x$ (parallel to the $x$-axis), magnetic field $H_z$ (parallel to the $z$-axis), and propagation coefficient $\beta$ are given by

$$\begin{pmatrix} E_x \\ H_z \end{pmatrix}\Big|_{\text{top air}} = \prod_m \begin{pmatrix} \cosh(\beta_m d_m) & \frac{j\omega\mu_0\mu_{zz}^m}{\beta_m}\sinh(\beta_m d_m) \\ \frac{\beta_m}{j\omega\mu_0\mu_{zz}^m}\sinh(\beta_m d_m) & \cosh(\beta_m d_m) \end{pmatrix} \times \begin{pmatrix} E_x \\ H_z \end{pmatrix}\Big|_{\text{bottom InP}}$$

$$\beta_m = \sqrt{(\mu_{zz}^m/\mu_{yy}^m)\beta^2 - k_0^2\varepsilon_{xx}^m\mu_{zz}^m}, \quad (1)$$

where $\varepsilon_{ij}^m$ and $\mu_{ij}^m$ are the $ij$ elements of the relative permittivity and permeability tensors in the $m$-th layer, respectively, and $d_m$ is the thickness of the $m$-th layer. At optical frequencies, the permeability tensors can be expressed by the identity matrix except in the SRR layer. Assuming an exponential decrease in $E_x$ and $H_z$ outside the core layer, we solved Eq. (1) and obtained the effective refractive index ($= \beta/k_0$) in each layer, as well as the transmission spectra in the device using the Fourier expansion method [14].

Figure 4(a) shows the calculated transmission spectra compared with the experimental data for the device with $350 \times 350$ nm SRRs. To fit the calculated spectra to the experimental ones, we set the effective thickness of the SRR region to 500 nm. Figure 4(b) shows the transmittance and reflectance spectra estimated for a row of SRRs. The insets in Fig. 4(b) visualize the distribution of electric field in an SRR at minimum transmission frequencies. This distribution shows that, at 1.55 $\mu$m band, the magnetic response of the SRR array is dominant in our device. Figure 4(c) shows the effective permeability (real and imaginary parts) of the SRR array, calculated as a function of frequency. The permeability exhibited a strong and sharp resonance at 200 THz, and the real part of the relative permeability changed from −0.7 to 2.7 around this frequency.

In summary, we demonstrated a device combining InP-based optical MMIs and an SRR-based metamaterial with a resonance wavelength at around 1.5 $\mu$m and nonunity relative permeability. Our results show the feasibility of semiconductor-based photonic devices combined with metamaterials. This design concept could be useful in the development of novel optical communication devices.

This research was financially supported by Grants-in-Aid for Scientific Research (19002009, 22360138, 21226010, 21860031, and 10J08973) from the Ministry of Education, Culture, Sports, Science, and Technology, Japan (MEXT).

## References

1. M. K. Smit, R. Baets, and M. Wale, in *IEEE Proceedings of the European Conference on Optical Communication* (IEEE, 2009), paper 1.7.3.
2. S. C. Nicholes, M. L. Masanović, B. Jevremović, E. Lively, L. A. Coldren, and D. J. Blumenthal, J. Lightwave Technol. **28**, 641 (2010).
3. H. J. Lezec, J. A. Dionne, and H. A. Atwater, Science **316**, 430 (2007).
4. W. Cai, U. K. Chettiar, H. K. Yuan, V. C. de Silva, A. V. Kildishev, V. P. Drachev, and V. M. Shalaev, Opt. Express **15**, 3333 (2007).
5. M. S. Rill, C. E. Kriegler, M. Thiel, G. von Freymann, S. Linden, and M. Wegener, Opt. Lett. **34**, 19 (2009).
6. I. V. Shadrivov, A. A. Sukhorukov, and Y. S. Kivshar, Phys. Rev. E **67**, 057602 (2003).
7. A. C. Peacock and N. G. R. Broaderick, Opt. Express **11**, 2502 (2003).
8. K. L. Tsakmakidis, A. D. Boardman, and O. Hess, Nature **450**, 397 (2007).
9. J. B. Pendry, A. J. Holden, D. J. Robbins, and W. J. Stewart, IEEE Trans. Microwave Theory Tech. **47**, 2075 (1999).
10. C. Enkrich, M. Wegener, S. Linden, S. Burger, L. Zschiedrich, F. Schmidt, J. F. Zhou, T. Koschny, and C. M. Soukoulis, Phys. Rev. Lett. **95**, 203901 (2005).
11. M. W. Klein, C. Enkrich, M. Wegener, C. M. Soukoulis, and S. Linden, Opt. Lett. **31**, 1259 (2006).
12. A. Ishikawa, T. Tanaka, and S. Kawata, J. Opt. Soc. Am. B **24**, 510 (2007).
13. T. Amemiya, T. Shindo, D. Takahashi, N. Nishiyama, and S. Arai, J. Quantum Electron. **47**, 736 (2011).
14. L. B. Soldano and E. C. M. Pennings, J. Lightwave Technol. **13**, 615 (1995).